ECS Journal of Solid State Science and Technology, **3** (5) P122-P125 (2014)
2162-8769/2014/3(5)/P122/4/$31.00 © The Electrochemical Society

Characterization of Ultra-Thin Ni Silicide Film by Two-Step Low Temperature Microwave Anneal

Chien-Ting Wu,[a,z] Yao-Jen Lee,[a,b] Fu-Kuo Hsueh,[a,c] Po-Jung Sung,[a,c] Ta-Chun Cho,[c] Michael Ira Current,[d] and Tien-Sheng Chao[c]

[a]*National Nano Device Laboratories, National Applied Research Laboratories, Hsinchu City, Taiwan*
[b]*Department of Physics, National Chung Hsing University, Taichung, Taiwan*
[c]*Department of Electrophysics, National Chiao Tung University, Hsinchu, Taiwan*
[d]*Current Scientific, San Jose, California 95124, USA*

A novel silicide process with two-step low temperature microwave annealing (MWA) achieves NiSi thickness of 10 nm while maintaining low resistance, and an ultra-thin Ni silicide film, only 4.5 nm, has been realized. In this MWA system, we insert quartz and Si susceptors to change the absorption efficiency of the process wafer and provide fine turning in temperature control during annealing. The thickness of NiSi film is determined by microwave power and by changing the number and the position of quartz and Si susceptors in the first step of the anneal process. The STEM-HAADF combined EELS/EDS spectroscopies are used to analyze the electronic excitations and identify the phase of Ni silicide.
© 2014 The Electrochemical Society. [DOI: 10.1149/2.006405jss] All rights reserved.

Manuscript submitted January 20, 2014; revised manuscript received February 20, 2014. Published March 6, 2014.

NiSi, a transition metal silicide, has been increasingly used for contacts in the latest complementary metal oxide semiconductor (CMOS) devices, owing to its low temperature of formation and low Si consumption during silicidation, low sheet resistance (R_S) and lower leakage current.[1,2] The use of NiSi currently faces a difficult trade-off between thickness and sheet resistance. The contact junction depth must still scale with gate length. To avoid high contact resistance and high contact leakage, no more than half the contact junction depth can be consumed in the formation of the silicide. Therefore, the silicide must become progressively thinner to accommodate the more shallow contact junction for scaled contacts. The rapid thermal annealing (RTA) has been widely used for silicidation and exhibits difficult thin-thickness and phase control. Microwave annealing (MWA)[3] has been realized to activate implanted dopants through solid phase epitaxial regrowth at low temperature.[4] It is promising for achieving advanced Si or Ge CMOS because of its unique volumetric heating and low temperature due to apparent non-thermal energy transfer.[5] The advantages of replacing rapid thermal annealing (RTA) with MWA are ultra-thin NiSi formation, diffusion-less junction, improved capacity of gate oxide and lower gate leakage. In this work, a novel two-step low temperature MWA process is used to form homogeneous NiSi contact films with low sheet resistance while not sacrificing thickness and quality.

During silicidation, many kinds of nickel silicide phases may appear simultaneously.[6] It has been reported that the predominant phases are Ni_2Si, NiSi and $NiSi_2$, form in the ranges 200–350, 350–750, and 750–1000°C, respectively.[7] The NiSi has the lowest resistivity among three different phases and other metal silicides. Furthermore, the Ni atoms are the primary moving species during the formation of NiSi phase. It could prevent the bridging effect which results in short circuit area between gate and source/drain.[8] It is well recognized that identification of nickel silicide phases after annealing is of crucial importance to its performance, especially, while these phases are formed in nano-polycrystalline layer. In this study, we use electron energy-loss spectroscopy[9–13] and energy dispersive X-ray spectroscopy[13,14] in conjunction with scanning transmission electron microscopy[14] (STEM-EELS/EDS) in order to identify the nickel silicide phases concentrating primarily on the Z-contrast image with atomic spatial resolution, elemental analysis, bulk plasmon excitaions and the chemical bonding.

Experimental

Two-step low temperature MWA.— Low resistance and ultra-thin NiSi is achieved by inserting quartz and Si susceptors above and below the process wafer during MWA. Figure 1 shows the schematic illustration of the MWA system. Si susceptors placed near the process wafer improve the uniformity of microwave energy absorption. The absorption of microwave power by quartz wafers is negligible. However, quartz wafers will absorb the heat from Si susceptors and help system to heat evenly. Therefore, quartz and Si susceptors change the absorption efficiency of the process wafer and provide fine turning in temperature control during MWA.

According to our experiments, the 10 nm Ni film shows better uniformity control of NiSi films than 5 nm Ni film. Moreover, when the thickness of Ni film decreases to 3 nm, it is easy to form a local $NiSi_2$ phase with a pyramidal structure penetrating into the underlying Si. A nominal 10 nm Ni film was pre-deposited on Si wafer by physical vapor deposition (PVD) with bias contact at the back side. Two-step annealing for NiSi layer formation was carried out by MWA processes. MWA uses a 5.8 GHz microwave source that results in heating of the bulk Si and Ni films. Each annealing step lasted for 300 sec.

A thin nickel silicide layer with partial crystallinity was formed by first MWA step. Then, we removed unreacted metal (Ni rich layer, Ni: >93%) by selective wet etching with H_2SO_4:H_2O_2 (3:1) solution at 120°C. After removing excess Ni, the second step MWA was performed. The thermal budget of the second step MWA is sufficient to transform the original partial-crystalline silicide into crystalline NiSi films with slightly increasing the silicide thickness.

STEM-EDS/EELS measurements.— In addition, our EELS/EDS work was carried out in a FEI (Tecnai F20; 200 kV) STEM capable of forming an electron probe as small as 0.2 nm and an energy

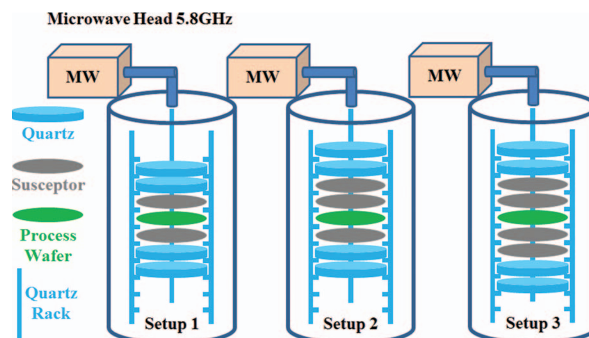

Figure 1. (Color online) Schematic illustration of the MWA system. Quartz and Si susceptors inside the chamber change the absorption efficiency of the process wafer.

[z]E-mail: ctwu@narlabs.org.tw

Downloaded on 2014-12-24 to IP 140.113.38.11 address. Redistribution subject to ECS terms of use (see ecsdl.org/site/terms_use) unless CC License in place (see abstract).

Table I. The summarized conditions of silicidation. All samples (A,B and C) use 10 nm Ni film and vary in power levels, one or two step MWA, and setup 1 versus setup 2.

	First-Step MWA		Second-Step MWA	
Sample	Setup 1	Setup 2	Setup 3	NiSi Thickness
A	600 W 240°C	–	1200 W 360°C	16 nm
B	–	600 W 196°C	1200 W 360°C	10 nm
C	540 W 233°C	–	1200 W 360°C	4.5 nm

resolution of ∼0.6 eV. With the 0.2 nm electron probe, we can explore the electronic excitation of an individual nano-object with high spatial resolution. The high-angle annular dark-field (HAADF) image with atomic spatial resolution (∼1 angstrom) was carried out in an aberration-corrected STEM (JEOL JEM 2100F).

Results and Discussion

A series of NiSi films (samples A,B and C) using MWA are performed and summarized in Table I. We supply different thermal budgets and setups in first-step MWA leads to various silicide thickness. All samples used the same optimum condition in setup 3 chamber with 1200 W microwave power in the second step annealing. 16 nm (sample A) and 10 nm (sample B) NiSi film are achieved by using setup 1 and setup 2 chambers, respectively, with 600 W microwave power in the first step MWA and followed by second-step MWA. The setup 1 chamber totally uses two Si susceptors and four quartz wafers above and below the process wafer. The setup 2 chamber added one more Si susceptor above the process wafer in order to absorb microwave energy and then reduce the process temperature. The maximum wafer surface temperatures in setup 1 and setup 2 chambers are 240°C and 196°C, respectively, as measured with a thermal label. The setup 3 chamber totally uses four Si susceptors and four quartz wafers above and below the process wafer with 1200 W microwave power. The maximum temperature on process wafer surface rises above 360°C as measured with an infrared thermometer from back-side (a thermal label showed a maximum temperature of about 300°C). Here, we note that the measured temperature should be considered as approximate due to the difficulties of temperature measurement in a microwave process chamber.

When MWA at 600 W was used with more than three Si suceptors, the resutling NiSi had poor thickness uniformity and mixed phases. A 4.5 nm NiSi film with very few $NiSi_2$ nano-islands, sample C, could be achieved by using setup 1 chamber with lower microwave power, 540 W, for the first step MWA. The maximum temperature on the process wafer surface is 233°C. Figures 2a ∼ 2e show the $[1\text{–}10]_{\text{Si substrate}}$ cross-sectional HRTEM images of thin silicide layers. Figure 2a shows a typical thin silicide layer with partial crystalline and unreacted Ni (on top) was formed by the first step MWA of sample B. After the second step MWA, silicide thickness is slightly increased from 9 nm to 10 nm. Figures 2b ∼ 2d show the HRTEM images of NiSi thin film samples A (16 nm), B (10 nm) and C (4.5 nm) after two-step MWA processes. In the HRTEM images, the large grain crystalline NiSi phase, without $NiSi_2$ penetration into Si could be observed and identified by its d-spacing.[15]

In our previous studies, a series of samples comparing two-step RTA/RTA, RTA/MWA and MWA/RTA anneals was carried out. According to these experiences, it is easy to form $NiSi_2$ phase with pyramidal structure penetrating into the underlying Si, as shown in Fig. 2e, after RTA or MWA process with higher thermal budget. Furthermore, while the thickness of nickel silicide reduces, a mixed $NiSi/NiSi_2$ phase is easy to form even for temperatures below 750°C. Low-temperature MWA process and the formation of a partially crystalline NiSi layer in the first step are the key to achieve the ultra-thin NiSi film without penetrating $NiSi_2$ phases. Furthermore, the thickness of NiSi film is determined by microwave power and by changing the number and the position of quartz and Si susceptors in the first step

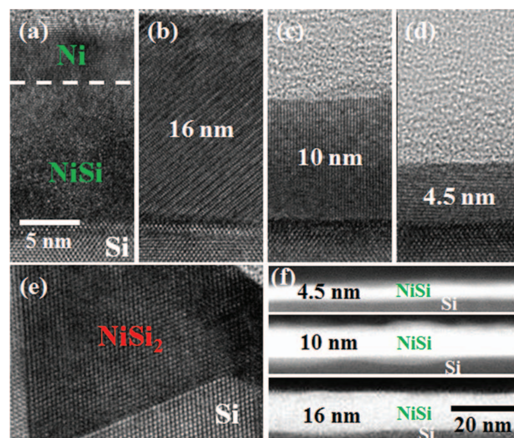

Figure 2. (Color online) HRTEM images and HAADF images of NiSi thin films. (a) A typical thin silicide layer with partial crystalline was formed by first step MWA of sample B. (b ∼ d) 16 nm, 10 nm and 4.5 nm NiSi thin films after two-step MWA. (e) A typical $NiSi_2$ phase with pyramids structure penetrating into the underlying Si after RTA or MWA process at higher temperature. (f) HAADF images of NiSi thin films with different thickness.

of the anneal process. Moreover, the uniformity of NiSi film could be improved by chamber design, such as wafer rotation during process with quartz susceptor-assisted.[16]

As the silicide thickness is pushed to below 10 nm after RTA or MWA process, in experience, it is easy to form nano structures with $NiSi_2$ phases in the silicide layer.[17–19] Figure 3 shows the $[1\text{–}10]_{\text{Si substrate}}$ high-resolution HAADF image of the 4.5 nm NiSi sample, with the brightest contrast signifying NiSi (green inset, Fig. 3) and the bright one in the right inset directing to $NiSi_2$ (red inset, Fig. 3) taking into account the weight sensitivity of the STEM-HAADF technique. It clearly shows a 4.5 nm NiSi thin film formed with a few, small and non-penetrating epi-$NiSi_2$ (10 ∼ 20 nm) regions at Si surface. These small $NiSi_2$ regions are not observed in 10 nm and 16 nm NiSi films. The volume fraction of $NiSi_2$ nano-island in 4.5 nm NiSi thin film is below 10%. By the HAADF imaging, lattice parameters of Si and $NiSi_2$ are similar (Si: 0.5430 nm, $NiSi_2$: 0.5406 nm),[13] and the in-plane mismatch between the atomic spacing on the $NiSi_2$ (111) and Si (111) planes is only 0.5%. Therefore a $NiSi_2$ layer is easy to form by epitaxial growth on Si(111) oriented substrates, as shown in right-insert figure in Fig. 3 with an epitaxial relation of $NiSi_2$ (111) // Si (111).[20]

In addition, the STEM combined EELS/EDS spectroscopies were also performed to identify the phase of nickel silicide. The Si elemental compositions of NiSi and $NiSi_2$ in Fig. 3 by STEM-EDS are

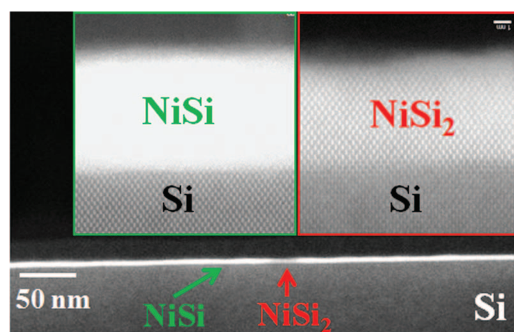

Figure 3. (Color online) The [110] cross-sectional HAADF image of 4.5 nm NiSi sample. In this imaging mode, the intensity of scattering scales with the atomic number Z as $Z^{1.7}$, so the brightest features are NiSi (left insert), the gray-white features are epi-$NiSi_2$ (right insert), and the Si substrates are weakly visible.

Downloaded on 2014-12-24 to IP 140.113.38.11 address. Redistribution subject to ECS terms of use (see ecsdl.org/site/terms_use) unless CC License in place (see abstract).

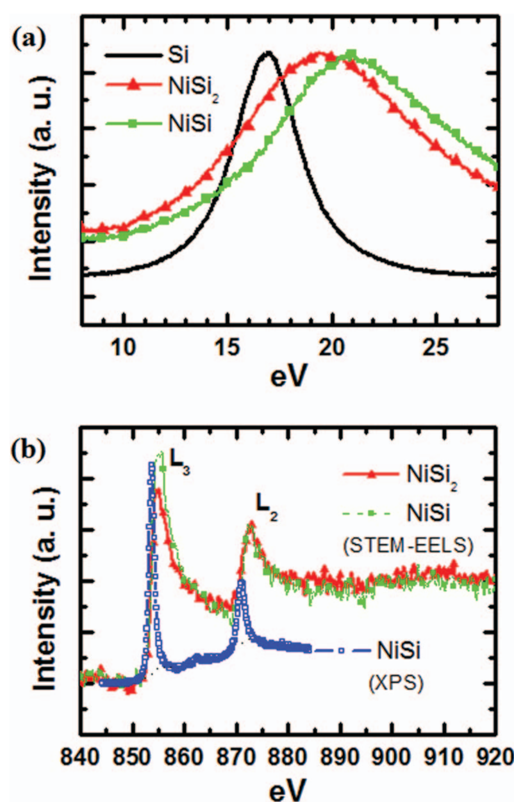

Figure 4. (Color online) (a) EELS low-loss spetra of Si, $NiSi_2$ and NiSi. (b) A typical XPS Ni-$L_{2,3}$ edge spectrum of NiSi film. And the ELNES Ni-$L_{2,3}$ edge spectra of $NiSi_2$ and NiSi films.

∼52% and ∼69%, respectively. Moreover, the Si elemental compositions in 10 nm and 16 nm NiSi films are 50% approximately. Fig. 4a shows portion of the STEM-EELS spectra taken across the interface with the electron probe pinpointing the observed Si, NiSi and $NiSi_2$, respectively. Upon positioning the electron probe at Si (Fig. 4a), we observed the characteristic bulk-plasmon excitation, 16.7 eV,[21,22] of the material. The readily observed bulk-plasmon excitations of $NiSi_2$ (19.7 eV) and NiSi (20.3 eV) in Fig. 4a are also nicely consistent with the known values of the respective materials,[10] in agreement with the STEM-EELS characterizations in Fig. 3. Furthermore, the variation of the binding energy of the Ni $L_{2,3}$ edge between pure nickel and nickel silicides are known to be 0.1 ∼ 1.9 eV (from Ni to Ni_3Si, $Ni_{31}Si_{12}$, Ni_2Si, NiSi, $NiSi_2$).[23,24] The chemical shifts of the Ni $L_{2,3}$ edge between NiSi and $NiSi_2$ is only 0.7 eV. However, there is no standard material, such as pure nickel, to be used as a reference for energy calibration in the sample. Therefore, the chemical shifts of core loss peaks are difficult to identify as NiSi and $NiSi_2$ phases. The branching (spin-orbit splitting) ratio of the $L_{2,3}$ edge is a candidate to be considered based on the information about oxidation state.[25] A typical X-ray photoelectron spectroscopy (XPS) spectrum of NiSi film is shown as an open-square (blue color) curve in Fig. 4b. The branching ratio can be calculated from the transition probability of $2p_{1/2}$ and $2p_{3/2}$ electrons to 3d orbits with background subtraction, and the ratio is 0.74 in agreement with the result of 0.75 ∼ 0.77 in previous studies.[11,26,27] In this study, the $NiSi_2$ phase is formed in small grain sizes in nanoscale which is difficult to obtain through XPS measurements due to its limited spatial resolution (∼15 μm). The spatially-resolved technique of STEM-EELS becomes an otherwise approach for studying the Ni-$L_{2,3}$ edge ELNES of such nano-scale phase, as shown in Fig. 4b. The dash-square (green color) and triangular-line (red color) curves in Fig. 4b are the Ni-$L_{2,3}$ edge ELNES spectra of NiSi and $NiSi_2$, respectively, after background subtraction and Fourier-ratio deconvolution of the plural scattering effects. The intensities had been

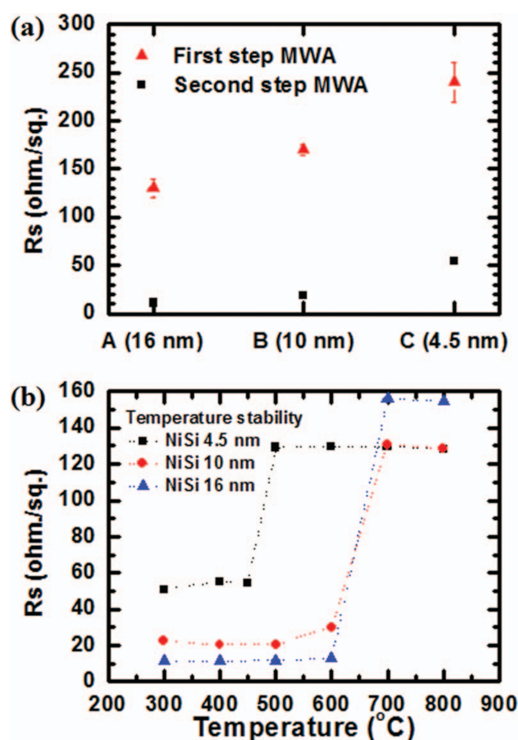

Figure 5. (Color online) (a) The variation of sheet resistance of NiSi thin film after one or two step MWA process using 10 nm Ni thin film. (b) The thermal stability of NiSi thin films of A (16 nm), B (10 nm) and C (4.5 nm) samples.

normalized to the L_2 maximum peak of each phase. It is clear that L_3 peak becomes smaller relative to the L_2 peak if the Si concentration increases. The branching ratio, which is defined as $I(L_3)/[I(L_2)+I(L_3)]$, of NiSi and $NiSi_2$ are 0.73 and 0.70, respectively, in agreement with the result of Asayama's work (NiSi: 0.74, $NiSi_2$: 0.68).[26]

After the first MWA step, the silicide thickness is extremely thin and the R_S is relatively high, as shown in Fig. 5a. After we apply a second MWA step, the R_S is markedly improved. The R_S of 16 nm, 10 nm and 4.5 nm NiSi films were reduced to 11, 18 and 50 ohm/sq. from 130, 170 and 240 ohm/sq., respectively. As expected, the thicker NiSi film has a lower R_S value. Furthermore, the higher sheet resistance of 4.5 nm-thick NiSi film should be attributed to more scattering for thinner film. Fig. 5b shows good thermal stability of NiSi films at least 450°C (4.5 nm NiSi) and 600°C (10 nm and 16 nm NiSi).

Conclusions

In conclusion, we demonstrate a novel silicidation process that forms NiSi thin films at a thickness of 10 nm while maintaining a low Rs. with two-step low temperature MWA. Using this method, an ultra-thin Ni silicide film, as thin as 4.5 nm, can be fabricated. The thickness of NiSi film is determined by microwave power and by changing the number and the position of quartz and Si susceptors in the first step of the anneal process. The STEM-HAADF combined with EELS/EDS spectroscopies are also performed to identify the phase of nickel silicide.

Acknowledgments

Helpful discussions with Professor C. H. Chen, Professor M. W. Chu, Dr. S. C. Liou and Dr. C.-P Chang for STEM-EELS are acknowledged. This work was supported by the National Science Council under the project of NSC grant Nos. 101- -2112-M-492-002-MY3.

Downloaded on 2014-12-24 to IP 140.113.38.11 address. Redistribution subject to ECS terms of use (see ecsdl.org/site/terms_use) unless CC License in place (see abstract).

References

1. T. Morimoto, T. Ohguro, S. Momose, T. Iinuma, I. Kunishima, K. Suguro, I. Katakabe, H. Nakajima, M. Tsuchiaki, M. Ono, Y. Katsumata, and H. Iwai, *Electron Devices, IEEE Transactions on*, **42**, 915 (1995).
2. J. A. Kittl, A. Lauwers, O. Chamirian, M. Van Dal, A. Akheyar, M. De Potter, R. Lindsay, and K. Maex, *Microelectron. Eng.*, **70**, 158 (2003).
3. Y.-J. Lee, L. Yu-Lun, H. Fu-Kuo, H. Kuo-Chin, W. Chia-Chen, C. Tz-Yen, H. Ming-Hung, J. M. Kowalski, J. E. Kowalski, H. Dawei, C. Hsi-Ta, L. Yiming, C. Tien-Sheng, W. Ching-Yi, and Y. Fu-Liang, *presented at the IEEE International Electron Devices Meeting* (2009).
4. L. Yu-Lun, H. Fu-Kuo, H. Kuo-Ching, C. Tz-Yen, J. M. Kowalski, J. E. Kowalski, Y.-J. Lee, C. Tien-Sheng, and W. Ching-Yi, *Electron Dev. Lett., IEEE*, **31**, 437 (2010).
5. J. H. Booske, R. F. Cooper, and I. Dobson, *J. Mater. Res.*, **7**, 495 (1992).
6. B. Cafra, A. Alberti, L. Ottaviano, C. Bongiorno, G. Mannino, T. Kammler, and T. Feudel, *Mater. Sci. Eng.: B*, **114–115**, 228 (2004).
7. M. Tinani, A. Mueller, Y. Gao, E. A. Irene, Y. Z. Hu, and S. P. Tay, *J. Vac. Sci. Technol. B:* **19**, 376 (2001).
8. H. Iwai, T. Ohguro, and S. Ohmi, *Microelectron. Eng.*, **60**, 157 (2002).
9. M. C. Cheynet and R. Pantel, *Micron*, **37**, 377 (2006).
10. T. H. Shohei Terada, Naoto Hashikawa, and Kyoichiro Asayama, *Jpn. J. Appl. Phys.*, **48**, 011203 (2009).
11. E. Verleysen, H. Bender, O. Richard, D. Schryvers, and W. Vandervorst, *J. Microsc.*, **240**, 75 (2010).
12. N. Kawasaki, N. Sugiyama, Y. Otsuka, H. Hashimoto, H. Kurata, and S. Isoda, *J. Appl. Phys.*, **109**, 063716 (2011).
13. N. Kawasaki, N. Sugiyama, Y. Otsuka, H. Hashimoto, M. Tsujimoto, H. Kurata, and S. Isoda, *Ultramicroscopy*, **108**, 399 (2008).
14. E. Verleysen, H. Bender, O. Richard, D. Schryvers, and W. Vandervorst, *J. Mater. Sci.*, **46**, 2001 (2011).
15. F. d'Heurle, C. S. Petersson, J. E. E. Baglin, S. J. L. Placa, and C. Y. Wong, *J. Appl. Phys.*, **55**, 4208 (1984).
16. Y.-J. Lee, H. Fu-Kuo, M. I. Current, W. Ching-Yi, and C. Tien-Sheng, *Electron Dev. Lett., IEEE*, **33**, 248 (2012).
17. J. Luo, Z. Qiu, C. Zha, Z. Zhang, D. Wu, J. Lu, J. Åkerman, M. Östling, L. Hultman, and S.-L. Zhang, *Appl. Phys. Lett.*, **96**, 031911 (2010).
18. Z. Zhang, S.-L. Zhang, B. Yang, Y. Zhu, S. M. Rossnagel, S. Gaudet, A. J. Kellock, J. Jordan-Sweet, and C. Lavoie, *Appl. Phys. Lett.*, **96**, 071915 (2010).
19. K. De Keyser, C. Van Bockstael, R. L. Van Meirhaeghe, C. Detavernier, E. Verleysen, H. Bender, W. Vandervorst, J. Jordan-Sweet, and C. Lavoie, *Appl. Phys. Lett.*, **96**, 173503 (2010).
20. U. Falke, A. Bleloch, M. Falke, and S. Teichert, *Phys. Rev. Lett.*, **92**, 116103 (2004).
21. C. H. Chen, J. Silcox, and R. Vincent, *Phys. Rev. B*, **12**, 64 (1975).
22. C.-T. Wu, M.-W. Chu, S.-B. Wang, M.-S. Hu, K.-H. Chen, L.-C. Chen, C.-W. Chen, and C. H. Chen, *Appl. Phys. Lett.*, **96**, 263106 (2010).
23. Y. Cao, L. Nyborg, and U. Jelvestam, *Surf. Interface Anal.*, **41**, 471 (2009).
24. P. L. Tam, Y. Cao, U. Jelvestam, and L. Nyborg, *Surf. Coat. Technol.*, **206**, 1160 (2011).
25. R. F. Egerton, *Electron Energy-Loss Spectroscopy in the Electron Microscope*, Plenum Press, New York (1996).
26. K. Asayama, N. Hashikawa, M. Kawakami, and H. Mori, in *Microscopy of Semiconducting Materials 2007*, A. G. Cullis and P. A. Midgley, Editor, Vol. 120, pp. 329-332, Springer Netherlands (2008).
27. E. Verleysen, H. Bender, D. Schryvers, and W. Vandervorst, *J. Phys.: Conf. Ser.*, **209**, 012057 (2010).

Downloaded on 2014-12-24 to IP **140.113.38.11** address. Redistribution subject to ECS terms of use (see **ecsdl.org/site/terms_use**) unless CC License in place (see abstract).